Construction and Building Materials 84 (2015) 253–260

Contents lists available at ScienceDirect

Construction and Building Materials

journal homepage: www.elsevier.com/locate/conbuildmat

Mechanical properties of hierarchically structured wood–cement composites

A. Quiroga [a], I. Rintoul [b,*]

[a] Universidad Tecnológica Nacional – Facultad Regional Santa Fe, Lavaise 610, S3004EWB Santa Fe, Argentina
[b] Instituto de Desarrollo Tecnológico para la Industria Química (INTEC UNL-CONICET), Universidad Nacional del Litoral – Consejo Nacional de Investigaciones Científicas y Técnicas, Ruta Nac.168 Km 472 Paraje "El Pozo", S3000GLN Santa Fe, Argentina

HIGHLIGHTS

- We model hierarchically structured materials.
- We model open cellular structured materials at the mesoscale.
- We model laminate structured materials at the microscale.
- We predict the mechanical properties of wood cement composites.

ARTICLE INFO

Article history:
Received 30 September 2014
Received in revised form 7 December 2014
Accepted 9 February 2015

Keywords:
Wood
Cement
Mechanical properties
Analytical modeling

ABSTRACT

Wood wool cement composites (WWCC) are widely used materials constituted of wood wool and Portland cement. The material presents excellent mechanical, chemical and biological properties. However, the understanding of its mechanical behavior is rather limited. In this contribution, a hierarchically structured model is presented to describe the mechanical behavior of WWCC under compressive stress. The material is modeled as 3D rigid open cellular structured material, 2D randomly oriented triple laminated material and particulated + fibrous material in the cm, mm and μm scales, respectively. The outcome of the model is a set of mathematical expressions permitting to predict the stress–strain behavior of the material in two cases: wood strands parallel and perpendicularly oriented to the stress direction. Mechanistically, the model predicts failure by buckling at the mesoscale. A statistical experimental work is included and used to validate the model.

1. Introduction

Composites are materials composed of a combination of two or more essentially non-miscible constituents that may differ in physical and chemical properties and/or in their structural or geometrical nature. Composite materials may present better properties than their original constituents. However, the number of possible combinations of constituents, ratios between them, ways of bonding, interface interactions, shape and relative orientation, among other variables make a real challenge to predict and design the properties of a composite even knowing the properties of their constituents [1]. The situation is particularly complex in case of composites with hierarchical levels [2].

Wood wool cement composites (WWCC) are widely used building materials constituted of wood wool (WW) and Portland cement (PC) [3]. The material is a rigid open cellular structure formed by strands of wood coated and bonded with set PC. Good mechanical properties, low density, high durability, dimensional stability, fire and water resistance, good acoustic and thermal insulation properties, resistance to biological and environmental degradation, low production costs and the possibility to easily vary their properties according specific needs are some of the most appreciated features of WWCC [4]. The driving forces for the study and research of WWCC is the replacement of asbestos based materials, the use of abundant and cheap cellulosic residues [5] and the replacement of organic adhesives such as phenols and formaldehydes commonly used in the production of particulated wood based materials [6]. Environmentally innocuous and cheap ceramic adhesives such as PC are of increasing interest [7,8].

The understanding of the mechanical and structural behavior of WWCC could contribute to improve and design its properties at the minimum cost [9]. The stiffness and strength of WWCC depend on the properties of wood and cement [10], the mineralization

* Corresponding author. Tel./fax: +54 342 4511370.
E-mail address: irintoul@santafe-conicet.gov.ar (I. Rintoul).

http://dx.doi.org/10.1016/j.conbuildmat.2015.02.091
0950-0618/

treatment of the wood [11], the density or compactness degree of the material [12] and the wood–cement ratio [13].

WWCC is a differentially structured material in the cm, mm and μm scales. A scheme of the material at different magnifications is presented in Fig. 1.

In the cm scale, the material may be classified as open cellular structured. Open cellular structured materials are two phase composites where each phase is continuous and interpenetrated by the other phase. Here, one phase is air and the other phase is a solid composite constituted of wood and cement. The air phase is named as macroporosity. The stiffness (E), the strength for crushing (σ^{crush}) and the strength for collapse (σ^{coll}) of an open cellular structured material are given by Eqs. 1–3 [14]:

$$E = E_s\, V_s^2 \tag{1}$$

$$\sigma^{crush} = 0.65\, \sigma_{f,s}\, V_s^{1.5} \tag{2}$$

$$\sigma^{coll} = 0.05\, E_s\, V_s^2 \tag{3}$$

Here, E_s is the stiffness, V_s is the volume ratio and $\sigma_{f,s}$ is the fracture strength of the solid phase of the open cellular structured material. V_s is defined as the volume of the solid phase divided the total volume of the open cellular structured material ($v_s\, V_T^{-1}$). V_T is the v_s plus the volume of the macroporosity ($v_s + v_{macro}$). Fig. 2 presents the compressive stress (σ) – strain (ε) behavior of open cellular structured materials.

In the mm scale, the solid composite of wood and cement happens to be structured as laminate where wood strands of several microns of thickness, a few millimeters wide and many centimeters long are coated and bonded by inorganic cement. This wood–cement sandwich composite can present certain degree of porosity. This porosity will be named as microporosity. In this case, the stiffness of the composite can be roughly described according to the Voigt and Reuss models presented in Eqs. (4) and (5), respectively [15]:

$$E_s^{Voigt} = E_w\, V_w + E_c\, V_c \tag{4}$$

$$E_s^{Reuss} = E_w\, E_c (E_w\, V_c + E_c\, V_w)^{-1} \tag{5}$$

Here, E_s^{Voigt} and E_s^{Reuss} are the stiffness of the composite when it is stressed parallel and perpendicular to the direction of the laminate, respectively. E_w, E_c, V_w and V_c are the stiffness and the volume fractions of wood and cement, respectively.

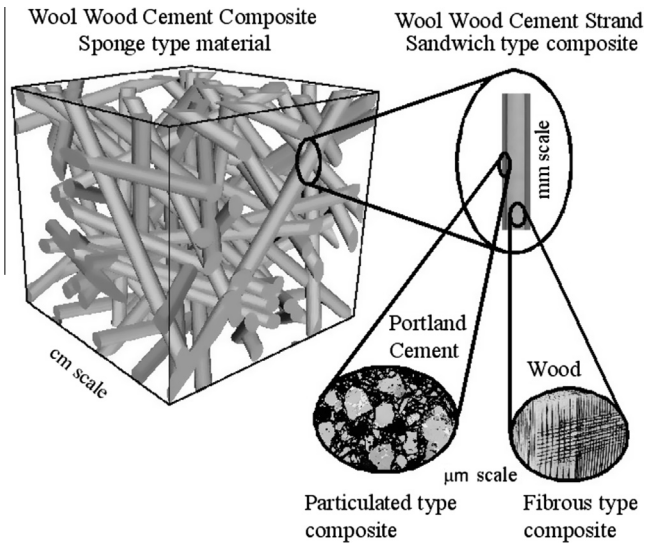

Fig. 1. Scheme of wood wool cement composites at different magnifications.

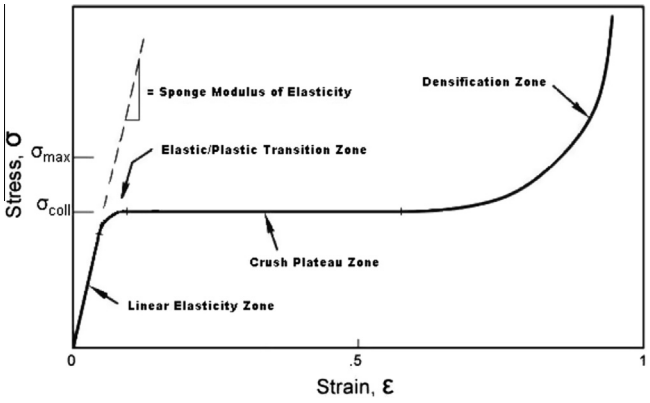

Fig. 2. Compressive stress–strain behavior of open cellular structured materials.

Finally, at the μm scale the fibrous and particulated structures of wood and cement can be identified. Wood is a composite mainly constituted of cellulose fibers and lignin. PC is a complex inorganic polycrystalline structure. Such structure is in the form of a hydraulic conglomerate of calcium, silica, aluminum, iron and magnesium oxides. The deduction of the wood and cement stiffness calculated from their basic constituents will not be included in this paper since it can be consulted in the works of Fratzl [16], Haecker [17] and Smilauer [18].

This contribution is devoted to the deduction and experimental validation of the hierarchically structured model proposed in Fig. 1 for WWCC and of a set of mathematical expressions for the stiffness and strength of an open cellular structured material whose solid phase is formed by a laminated structure with constituents of very different properties i.e. wood: low stiffness – high toughness and PC: high stiffness – low toughness.

2. Materials and methods

2.1. Materials

WW of sapwood of Populus X Euroamericana CV harvested in the northeastern of Argentina and Portland cement CPN40 IRAM 50.000 (Minetti, Argentina) were selected as materials. The density of Populus X Euroamericana CV (δ_w) and set Portland cement CPN40 IRAM 50.000 (δ_c) are 0.405 g cm^{-3} [19] and 2.0 g cm^{-3} [20], respectively. Populus X Euroamericana CV is a fast growing tree species implanted in forest areas of Argentina. Technical grade calcium chloride, $CaCl_2$, (Cicarelli, Argentina) was used as setting accelerator. Distilled water was used for the extraction of setting inhibitory substances naturally present in the sapwood and for the cement paste preparation. Paraffin wax (Induquimika, Argentina) with 50 °C of melting point and 0.845 g cm^{-3} of density ($\delta_{paraffin}$) [21] was used for the determination of V_s. Demineralized water was used for wood treatments and clinker hydratation. Acrylic resin (Induquimika, Argentina) was used for the preparation of samples for microscope observation.

2.2. Preparation of WWCC specimens

Setting inhibitory substances such as sugars and hemicelluloses were extracted from the wood. A sample of 450 g of WW was immersed into a water bath at 100 °C during 30 min. The H_2O/WW ratio was 40 g g^{-1}. Subsequently, the WW sample was removed from the bath and dried in an oven at 105 °C until constant weight. This process is absolutely necessary to permit the correct setting of PC on the wood surface [22].

A cement paste was prepared mixing 1200 g of PC, 700 g of water and 60 g of $CaCl_2$. Immediately after, the cement paste was homogeneously distributed over the surface of 450 g of treated WW. The resulting mixture was placed into a mold of 30 × 30 × 7 cm^3 size. The setting reaction was left to proceed during 72 h in a controlled environment chamber set at 100% humidity and 25 °C. After this period, the mold was open to obtain a WWCC board. The board was dried in a ventilated stove set at 50 °C. The board reached constant weight after 24 h of drying. Finally, it was cut in 16 cubic samples of 7 cm side. The procedure was repeated ten times to ensure good statistical and representative results. In total 160 specimens were obtained. However, only the 4 central specimens of each board were used for different tests. The 12 peripheral specimens of each board were rejected. This selection permitted to eliminate border anomalies commonly observed in molded materials.

The development of the model was carried out using information from WWCC specimens obtained according the above described procedure.

Variations of the above described procedure were performed to validate the applicability of the model to a broader range of WWCC conditions. Specifically, the validation of the model in terms of WW/PC weight ratio and density were verified. The WW/PC ratio was varied from 0.250 to 0.500 by modifying the amount of PC, from 1200 g of PC to 1800 g and 900 g of PC, respectively and proportionally, the amounts of $CaCl_2$ and H_2O, of the above described recipe while keeping constant the other conditions. The density of the WWCC was varied from 320 kg m^{-3} to 160 kg m^{-3} by doubling the molding volume, from $30 \times 30 \times 7$ cm^3 to $30 \times 30 \times 14$ cm^3 while keeping constant the other conditions. The procedures for model validation were performed in triplicate to ensure representative results.

2.3. Macro and microstructure characterization

An optical microscope Leica DM 2500 M (Leica Microsystems, Germany) powered with Leica Application Suite Version 2.8.1. software was used for the observation of WWCC structures at different levels. Samples for microscopy were prepared. Slices of 1 cm from WWCC specimens were cut, dust was removed and were immersed in a liquid resin. After solidification, they were polished for microscopic observation.

2.4. Mechanical characterization of WWCC

Compression trials in WWCC were performed in a testing machine Instron 1137 (Illinois, USA). The crosshead speed was set at 0.20 mm s^{-1} for all tests. Consequently, the strain rate applied to the WWCC specimens resulted 2.85 10^{-3} s^{-1}. Ten specimens were tested in the direction parallel to the molding plane. $E_{//}$, $\sigma_{//}^{crush}$, $\varepsilon_{//}^{crush}$ and $\sigma//^{coll}$ were measured for each specimen. Here, $E_{//}$, $\sigma_{//}^{crush}$, $\varepsilon_{//}^{crush}$ and $\sigma_{//}^{coll}$ are the elasticity modulus, the stress for crushing, the deformation at the crushing point and the resistive stress during collapse, respectively. Another ten specimens were compressed in the direction perpendicular to the molding plane. $E_{\perp}$, $\sigma_{\perp}^{crush}$, $\varepsilon_{\perp}^{crush}$ and $S_{\perp}^{coll}$ were measured for each specimen. Here, $E_{\perp}$, $\sigma_{\perp}^{crush}$, $\varepsilon_{\perp}^{crush}$ and $S_{\perp}^{coll}$ are the elasticity modulus, the maximal stress or stress for crushing, the deformation at the crushing point and the slope for collapsing, respectively. All tests were carried out at 23 °C and at 50% of relative humidity.

2.5. Determination of V_s in WWCC specimens

V_s was determined by two methods: the paraffin method giving $V_s^{paraffin}$ and the water method giving V_s^{water}. Paraffin and water determinations were performed in fivefold. Ten specimens of WWCC of 7 cm^3 were dried in an oven set at 105 °C until constant weight. The volume (V_{wwcc}) and the weight (W_{wwcc}) of each specimen were recorded.

For the $V_s^{paraffin}$ determination, five dried specimens were immersed in a paraffin bath at 90 °C to seal the open microporosity by coating the laminated wood cement composite. Most of the macroporosity of the material remained open. The specimens were removed from the paraffin bath and left to drain the excess of paraffin. The specimens were cooled down and weighted ($W_{wwcc}^{paraffin}$). Finally, each specimen with sealed microporosity was immersed in water at 20 °C. $V_s^{paraffin}$ resulted from the ratio between the displaced water volume (V_{displ}) corrected by the extra volume of paraffin ($V_{paraffin} = (W_{wwcc}^{paraffin} - W_{wwcc})\,\delta_{paraffin}^{-1}$) to the V_{wwcc}. The macroporosity volume (V_{macro}) was calculated as $V_{wwcc} - V_{displ}$.

For the V_s^{water} determination, the other five dried specimens were completely immersed in water at 20 °C. Each 2 h the specimens were withdrawn from the water bath, the excess of water was left to drain during 10 min, the drained specimens were weighted and re-immersed into the water bath. The sequence was repeated 8 times until constant weight of the specimens after the draining step (W_{wwcc}^{water}). In this situation, the open microporosity of the WWCC could be considered as filled with water. Subsequently, the specimens were removed from the water bath, left to drain the excess of water and immersed into another water bath thermostated at 20 °C for measuring the liquid displacement. The displaced volume (V_{displ}) is the volume of the solid fraction of the WWCC including its microporosity, i.e. V_s^{water} resulted from the ratio between the displaced water to the V_{wwcc}. The microporosity volume (V_{micro}) was calculated as $(W_{wwcc}^{water} - W_{wwcc})\,\delta_{water}^{-1}$.

2.6. Mechanical characterization of WW

Individual WW strands were tested in an Instron 3344 (Illinois, USA) machine for determination of WW stiffness (E_w). Ten samples of 30 wood strand specimens were tested totalizing 300 stiffness measurements. The distance between clamps was set at 2 cm, the samples were stressed with a force of 1 N previous to the test to fit the WW in the clamps. The strain rate was 5 mm min^{-1}. The average linear density of WW was determined. In addition, the average width and the average thickness of the strands were determined using a Precision Micrometer (Testing Machines Inc., USA). 30.0 g of WW were unwinded and every strand was measured in length, width and thickness. The width and the thickness were measured several times per strand. All tests and geometrical measurements were carried out at 23 °C and at 50% of relative humidity.

2.7. Mechanical characterization of Portland cement

The compressive strength of set PC was determined according to the procedure described in ASTM C109/C109M – 11a Standard Test Method for Compressive Strength of Hydraulic Cement Mortars (Using 50-mm Cube Specimens). The test was repeated five times to ensure confidential results. Water with some content of wood extractives was used to simulate the conditions for setting of PC on the wood surface. The water solution was prepared by extraction of 30 g of WW in 300 g of water during 2 h at 25 °C. E_c was calculated using Eq. (6) [23]:

$$E_c = 33\,\delta_c^{1.5}\sigma_c^{0.5} \tag{6}$$

Here, σ_c is the compressive strength of PC.

2.8. Determination of V_w and V_c in WWCC

Five specimens of WWCC of 7 cm^3 were dried at 105 °C until constant weight. The weight of the dried samples was recorded as W_{wwcc}. Subsequently, the samples were burned in an oxidizing atmosphere at 400 °C during 12 h. Such conditions permitted to burn the organic phase of the samples preserving the inorganic PC phase and including its hydraulic content, $CaCl_2$ and the minerals naturally present in the wood. The weight after burning was recorded as W_{wwcc}^{burn}. V_w and V_c were calculated using Eqs. (7) and (8):

$$V_w = W_w\,\delta_w^{-1} \tag{7}$$

$$V_c = W_c\,\delta_c^{-1} \tag{8}$$

where:

$$W_w = W_w^{organic} + W_w^{inorganic} \tag{9}$$

and

$$W_w^{organic} = W_{wwcc} - W_{wwcc}^{burn} \tag{10}$$

$$W_w^{inorganic} = \left(W_{wwcc} - W_{wwcc}^{burn}\right) wt\%^{inorganic}\; wt\%^{inorganic-1} \tag{11}$$

$$W_c = W_{wwcc}^{burn} - W_w^{inorganic} \tag{12}$$

$wt\%^{inorganic}$ and $wt\%^{organic}$ were obtained from weight differences of WW samples before and after burning. Five samples of WW of 30.0 g were dried at 105 °C until constant weight. 30.0 g was the needed amount of WW to produce a WWCC specimen of 7 cm^3 identical to those used in the precedent procedure. The weight of the dried samples was recorded as W_{ww}. Subsequently, the samples were burned in an oxidizing atmosphere at 400 °C during 12 h. The weight after burning was recorded as W_{ww}^{burn}. Finally:

$$wt\%^{inorganic} = 100\,W_{ww}^{burn}\,W_{ww}^{-1} \tag{13}$$

$$wt\%^{organic} = 100\left(W_{ww} - W_{ww}^{burn}\right) W_{ww}^{-1} \tag{14}$$

3. Results

3.1. Macro and micro structure of WWCC

A picture of a typical WWCC specimen of 7 cm^3 is shown in the upper left corner of Fig. 3. Face "a" of the specimen is identified as the molding plane and the molding direction is perpendicular to the molding plane. Faces "b" and "c" are identified as the lateral views of the specimen. In the upper right corner of Fig. 3 a top view of the molding plane and a lateral view of the specimen are presented. A magnified lateral view of the specimen is presented in the lower left corner of Fig. 3. Here, the cutting tails of the strands are observed. There is no observation of strands oriented perpendicular to the molding plane. The material presents an open cellular structure with macroporous in the order of several mm. The body seems to be formed by homogeneous bonded strands, 2D randomly oriented and parallel to the molding plane. A small angle (β) between the plane of 2D wood strands orientation and the molding plane can be observed to the naked eye. The β angle was measured in several planes along the sample using a protractor. The average β angle resulted 0.17 rads. In addition, the strand gap between bonds (L) was systematically measured 400 times. The arithmetic

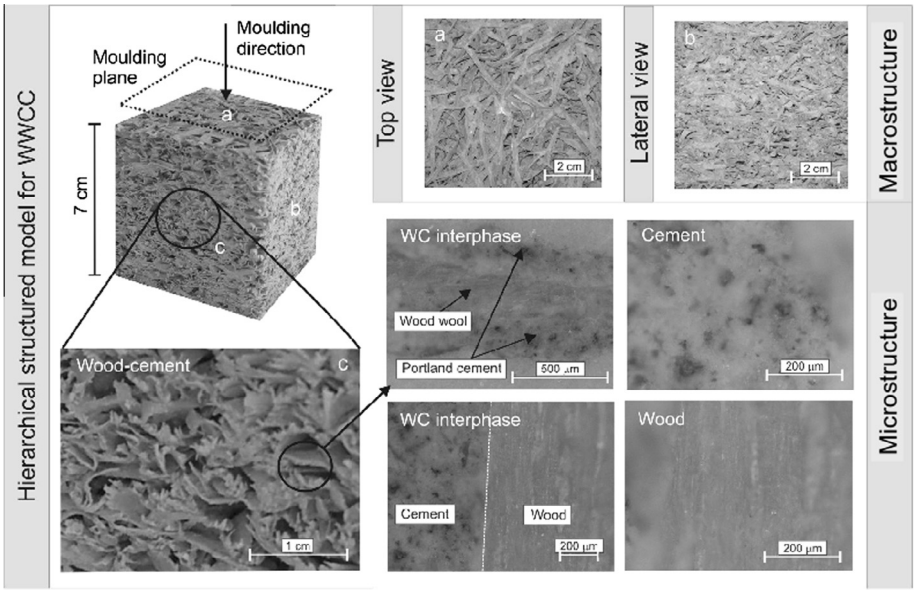

Fig. 3. Structure of WWCC at different magnification levels.

average strand gap resulted $L = 0.007$ m. Four micrographs of WWCC are shown in the lower right side of Fig. 3. Here, the constitution of the strands is appreciable. Clearly, the strands are formed by a soul of wood coated by set PC. Laminate structures can be identified. In addition, a detail showing the wood cement interface is presented and the particulated hydraulic conglomerate structure of PC and fibrous wood structures are also exposed. Fig. 3 validates the graphical model presented in Fig. 1.

3.2. Mechanical characterization of WWCC

Fig. 4 shows typical stress–strain plots for WWCC compression parallel and perpendicular to the molding plane.

Four zones can be identified in the stress–strain plot for compression parallel to the molding plane: the linear elasticity zone, the crushing zone, a collapsing plateau and the densification zone. Three zones can be identified in the stress–strain plot for compression perpendicular to the molding plane: the linear elasticity zone, a nearly linear collapsing zone and the densification zone. The very different typology of the stress–strain plots for compression parallel and perpendicular to the molding plane suggests high anisotropy of the structure of the material and different mechanistic responses to compression. Table 1 summarizes the obtained results.

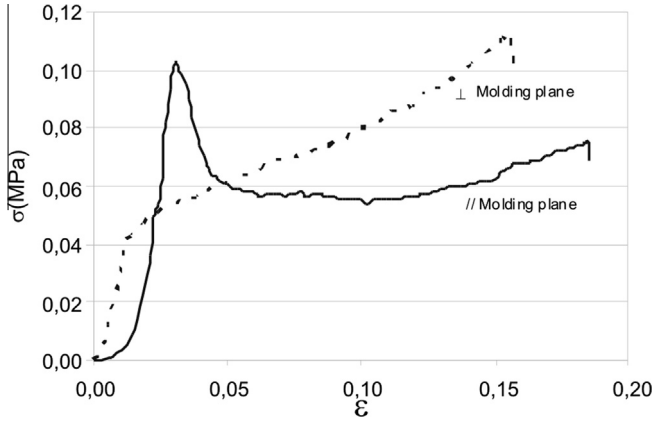

Fig. 4. Stress–strain plots for WWCC tested in the direction parallel (full line) and perpendicular (dashed line) to the molding plane.

The average of the absolute deviation of the WWCC densities resulted 4.61 representing 1.43% over an average density value of 322 kg m^{-3}, thus confirming good reproducibility during the formulation, board synthesis and specimens preparation procedures. The average of the absolute deviation of WWCC $E_{//}$, $\sigma_{//}^{crush}$, $\varepsilon_{//}^{crush}$, $\sigma_{//}^{coll}$, $E_{\perp}$, $\sigma_{\perp}^{crush}$, $\varepsilon_{\perp}^{crush}$ and $S_{\perp}^{coll}$ were 0.15, 0.010, 0.001, 0.012, 0.06, 0.005, 0.006 and 0.01, respectively. Those values represent 15%, 10%, 7% 17%, 23%, 12%, 28% and 13% of the resulting average values. The values are acceptable considering the high anisotropy and the non-homogeneous nature of the material.

$E_{//}$ resulted almost 4 times higher than $E_{\perp}$ and $\sigma_{//}^{crush}$ resulted double than $\sigma_{\perp}^{crush}$. However, $\varepsilon_{//}^{crush}$ and $\varepsilon_{\perp}^{crush}$ resulted identical. Interestingly, the material absorbs energy after crushing. $\sigma_{//}^{coll}$ remains at 70% of $\sigma_{//}^{crush}$ along a deformation of near 5 times $\varepsilon_{//}^{crush}$. After that, σ increases exponentially. In case of compression perpendicular to the molding plane, the compressive strength increases almost linearly after crushing with a rate of $S_{\perp}^{coll}$ along a deformation of near 5 times $\varepsilon_{\perp}^{crush}$. After, σ increases exponentially.

3.3. Determination of V_s in WWCC specimens

Table 2 presents the results of the paraffin and the water methods used to determine V_s. The average of the absolute deviation between $V_s^{paraffin}$ and V_s^{water} values resulted 0.020 and 0.024

Table 1
Results for WWCC specimens tested under compression parallel (//) and perpendicular (⊥) to the molding plane.

Sample		Compression parallel to the molding plane				Compression perpendicular to the molding plane			
N°	δ_{wwcc} kg m^{-3}	$E_{//}$ MPa	$\sigma_{//}^{crush}$ MPa	$\varepsilon_{//}^{crush}$	$\sigma_{//}^{coll}$ MPa	$E_{\perp}$ MPa	$\sigma_{\perp}^{crush}$ MPa	$\varepsilon_{\perp}^{crush}$	$S_{\perp}^{coll}$ MPa
1	331	1.03	0.112	0.021	0.078	0.23	0.046	0.020	0.04
2	326	0.82	0.074	0.021	0.040	0.22	0.034	0.015	0.04
3	326	1.09	0.104	0.021	0.076	0.27	0.040	0.014	0.04
4	317	0.61	0.076	0.021	0.060	0.32	0.046	0.024	0.04
5	326	1.31	0.104	0.017	0.104	0.28	0.048	0.021	0.03
6	323	0.89	0.102	0.020	0.078	0.36	0.050	0.014	0.05
7	323	1.23	0.102	0.017	0.086	0.15	0.038	0.031	0.04
8	321	0.93	0.112	0.019	0.064	0.13	0.036	0.032	0.03
9	320	0.98	0.106	0.019	0.070	0.28	0.044	0.014	0.05
10	306	1.09	0.106	0.021	0.068	0.33	0.052	0.015	0.05
Av	322	1.00	0.100	0.020	0.072	0.26	0.043	0.020	0.04

Table 2
Determination of micro and macro porosities and the volume ratio of solid in WWCC.

Paraffin method	V_{wwcc} ml	W_{wwcc} g	$W_{wwcc}^{paraffin}$ g	V_{displ} ml	$V_{paraffin}$ ml	V_{macro} ml	$V_s^{paraffin}$
1	324	105	162	189	67	202	0.38
2	319	89	148	177	66	208	0.35
3	321	95	146	177	55	199	0.38
4	322	100	140	182	44	184	0.43
5	320	96	158	185	69	204	0.36
Av	321	97	151	182	60	199	0.38
Water method	V_{wwcc} ml	W_{wwcc} g	W_{wwcc}^{water} g	V_{displ} ml	V_{micro} ml	V_{macro} ml	V_s^{water}
1	343	96	174	139	77	204	0.41
2	348	102	183	139	81	209	0.40
3	343	98	171	138	73	205	0.40
4	348	107	193	154	86	194	0.44
5	333	102	189	154	87	179	0.46
Av	343	101	182	145	81	198	0.42

representing near 5% and 6%, respectively over average values of $V_s^{paraffin} = 0.38$ and $V_s^{water} = 0.42$. The paraffin method gives V_s nearly 10% lower than the water method. Such difference can be considered as acceptable. $V_s = 0.4$ implies that near 40% of the WWCC volume is solid and 60% is air in the form of open macroporosity.

3.4. Mechanical characterization of WW

The average E_w over 300 tested strands resulted 1500 MPa. Table 3 summarizes the average E_w value for each of the 10 wood strand samples. The normal dispersion on E_w measurements was 13%. The highest and the lowest E_w were 7900 MPa and 200 MPa, respectively. In addition, the difference between the highest and the lowest E_w measured within one sample of 30 strands could be as high as 7400 MPa. As observed, highly dispersed values were obtained in E_w determinations. Therefore, a high number of strands had to be tested to get reliable information about the properties of WW.

30.0 g of WW resulted a total length of about 30 m. Then, the linear density of WW was calculated as 1 g m^{-1}. The average width (a) and the average thickness (e) resulted 3.0 mm and 0.2 mm, respectively. The lowest area moment of inertia (I) of the strand was calculated as $I = a\,e^3\,12^{-1}$. Then, $I = 1.85\ 10^{-15}$ m^4.

3.5. Mechanical characterization of Portland cement

The average σ_c resulted 39 MPa. Table 4 summarizes all the results. E_c was obtained according to Eq. (6). $E_c = 18400$ MPa.

3.6. Volume fraction of wood (V_w) and cement (V_c) in WWCC

Table 5 shows the volume fractions of wood and cement in WWCC and the wt% of organic and inorganic phases in the wood.

Table 3
Elasticity modulus of wood strands.

Sample N°	E_w MPa
1	1100
2	1600
3	1300
4	1600
5	1800
6	1600
7	2100
8	1900
9	1700
10	1200
Av	1500

Table 4
Compression strength and stiffness of PC.

Sample N°	σ_c MPa	E_c MPa
1	43	19300
2	36	17600
3	46	20100
4	39	18500
5	32	16600
Av	39	18400

Table 5
Volume fraction of wood (V_w) and cement (V_c) in WWCC and weight percentage of organic ($wt\%^{organic}$) and inorganic ($wt\%^{inorganic}$) in the wood.

Sample N°	W_{wwcc} g	W_{wwcc}^{burn} g	V_w	V_c
1	95	67	0.68	0.32
2	80	55	0.69	0.31
3	99	71	0.67	0.33
4	78	56	0.66	0.34
5	80	66	0.68	0.32
Av	87	63	0.68	0.32
Sample N°	W_{WW} g	W_{WW}^{burn} g	$wt\%^{organic}$	$wt\%^{inorganic}$
1	30	0.27	99.1	0.89
2	30	0.28	99.1	0.93
3	30	0.36	98.8	1.20
4	30	0.39	98.8	1.30
5	30	0.30	99.0	0.98
Av	30	0.32	98.9	1.10

3.7. Mechanical characterization of WWCC used for model validation

The mechanical characterization of WWCC specimens used for the validation of the model in a broader range of WWCC conditions was carried out as described in Section 3.2. The most relevant properties for industrial applications were measured, i.e. $E_{//}$, $\sigma_{//}^{crush}$, $E_\perp$ and $\sigma_\perp^{crush}$. Table 6 presents the results.

The arithmetic average of the measured properties were calculated. $E_{//} = 1.50$ MPa, $\sigma_{//}^{crush} = 0.170$ MPa, $E_\perp = 0.677$ MPa and $\sigma_\perp^{crush} = 0.078$ MPa resulted as averaged values of WWCC specimens obtained with WW/PC = 0.250 while keeping constant the other conditions. $E_{//} = 0.55$ MPa, $\sigma_{//}^{crush} = 0.069$ MPa, $E_\perp = 0.165$ MPa and $\sigma_\perp^{crush} = 0.028$ MPa resulted as averaged values of WWCC specimens obtained with WW/PC = 0.500 while keeping constant the other conditions. Finally, $E_{//} = 0.045$ MPa, $\sigma_{//}^{crush} = 0.018$ MPa, $E_\perp = 0.026$ MPa and $\sigma_\perp^{crush} = 0.015$ MPa resulted as averaged values of WWCC specimens obtained doubling the molding volume while keeping constant the other conditions.

Clearly, the increment of the PC content, and proportionally, the amounts of $CaCl_2$ and H_2O, increases $E_{//}$, $\sigma_{//}^{crush}$, $E_\perp$ and $\sigma_\perp^{crush}$. Oppositely, the increment of the molding volume decreased

Table 6
Results for WWCC specimens tested under compression parallel (//) and perpendicular (⊥) to the molding plane.

WW/PC	Molding volume m^3	$E_{//}$ MPa	$\sigma_{//}^{crush}$ MPa	$E_\perp$ MPa	$\sigma_\perp^{crush}$ MPa
0.250	0.0063	1.64	0.166	0.63	0.089
0.250	0.0063	1.23	0.178	0.82	0.079
0.250	0.0063	1.64	0.167	0.58	0.065
0.500	0.0063	0.55	0.084	0.15	0.025
0.500	0.0063	0.51	0.062	0.18	0.030
0.500	0.0063	0.59	0.062	0.17	0.027
0.375	0.0126	0.02	0.023	0.02	0.020
0.375	0.0126	0.02	0.013	0.02	0.015
0.375	0.0126	0.01	0.018	0.01	0.011

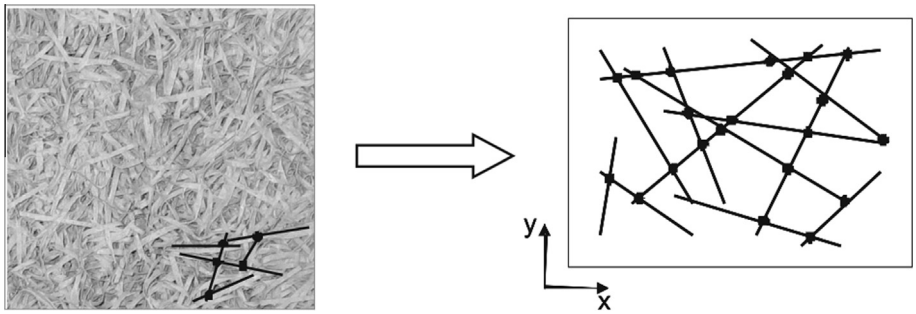

Fig. 5. Conceptual simplification of the 2D randomly oriented strand structure.

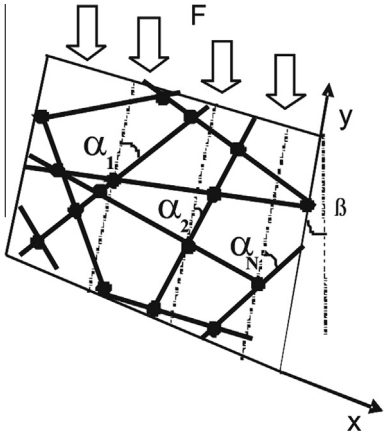

Fig. 6. Scheme of force action on a conceptual segments-nodes network proposed as model for a WWCC material tested under compression parallel to the molding plane.

$E_{//}$, $\sigma_{//}^{crush}$, $E_{\perp}$ and $\sigma_{\perp}^{crush}$. The great anisotropy observed in precedent results seems to be diminished since $E_{//} \sim E_{\perp}$ and $\sigma_{//}^{crush} \sim \sigma_{\perp}^{crush}$. Visually, the WWCC shows higher macroporosity and the strands are almost randomly oriented. The visual difference between parallel and perpendicular molding directions is practically null.

4. Discussion

4.1. Validation of the hierarchical structure of WWCC

Figs. 3 confirms the hierarchical structure of WWCC proposed in Fig. 1. Clearly, the resulted composite seems an open cellular structured material whose solid phase appears in the form of laminate composite of cement and wood. High anisotropy and porosity of the macrostructure is evident. The 2D orientation of the strands in the molding plane is due to the effect of constrain and press down during the molding process. The WW/PC interface seems firm and compact. The small β angle between the plane of 2D wood strands orientation and the molding plane can be assigned to the procedure of mold filling. In this process an undefined paste of WW and PC is distributed into the mold cavity. Non-homogeneous distribution of the WW–PC paste is common.

4.2. Mechanical behavior of WWCC

The very different typology of the stress–strain plots for compression parallel and perpendicular to molding directions confirms the high anisotropy of the material structure and suggests different mechanistic responses to compression. Compression parallel and perpendicular to the molding direction suggests buckling of the slender strands composing the WWCC body. It is important to note that the WWCC samples of 7 cm^3 used for compressive tests did not suffer buckling effect and the material body behaves as a whole piece. In addition, this buckling suggestion may be in agreement with the observed difference between $E_{//}$ and $E_{\perp}$ and the difference between $\sigma_{//}^{crush}$ and $\sigma_{\perp}^{crush}$. The fact that $\varepsilon_{//}^{crush}$ and $\varepsilon_{\perp}^{crush}$ resulted almost identical may also suggest that the ultimate resistance for crushing is also affected by a parameter independent of the strands orientation and the molding and stress directions. Detachment of the WW/PC interface and cracking of the PC coating on the wood surface are proposed to explain this behavior.

4.3. Solid volume ratio and volume fraction of wood and cement in WWCC specimens

As mentioned above, a V_s of 0.4 in the WWCC implies that near 40% of the material volume is solid and 60% is air in the form of open macroporosity. In addition, V_w and V_c can be approximated to 0.7 and 0.3, respectively. Therefore, the 70% of the solid part of the WWCC is wood.

4.4. Mechanical characterization of WW and PC

The high dispersion in E_w can be assigned to the fact that wood strands are obtained from different parts of the tree. Moreover, the axes of the raw wood slabs introduced into the stranding machine are not perfectly oriented to the direction of the stranding cutters. The relative low σ_c can be explained in terms of the setting inhibitory effect of wood extractives in the used water during the clinker hydration process. It is well known that sugars and hemicelluloses impair the right clinker hydration resulting in a significant decrease of the final properties of PC.

4.5. Hierarchical model development

The left side of Fig. 5 presents a magnified view of the molding plane of a WWCC specimen. Clearly, the strands are 2D randomly oriented, coated and bonded with PC. The real system is suggested to be understood as a simplified network of rigid sticks linked together as shown in the right side of Fig. 5. The plane where the 2D randomly oriented strands lies is named as plane y–x.

Every stick in the network is bonded to other sticks. Each bond acts as a node and the part of the stick between two nodes act as a segment. Therefore, the proposed simplified network can actually be understood as a model network composed of N segments and M nodes. Moreover, as most of the segments are between two nodes and every node is shared by four segments, then: $N = 2M$. N was estimated for a 7 cm^3 specimen prepared for compression test. Each board of $30 \times 30 \times 7$ cm^3 is composed of near 450 g of WW. Therefore, each one of the 16 specimens of 7 cm^3 is composed of near 28 g of WW. The total strand (or eventually segment)

Table 7
Hierarchically structured model and experimental results.

Parameter	Model value MPa	Experimental value Mpa	Deviation %
$\sigma_{//}^{crush}$	0.096	0.100	4
$\sigma_{\perp}^{crush}$	0.050	0.043	16
$E_{//}$	0.89	1.00	11
$E_{\perp}$	0.30	0.26	15
$\sigma_{//}^{coll}$	0.054	0.072	25

length (H) in a 7 cm^3 specimen can be estimated as the ratio between those 28 g of WW and the linear density of the wood strands (1 g m^{-1}). H is 28 m. N is calculated as $H\ L^{-1}$. Then, $N \sim 4000$. The force (F) capable to resist the model network is the sum of the individual resistance forces of the segments (f_i):

$$F = \sum_{i=1}^{N} (f_i) \tag{15}$$

The quantification of each f_i is not an easy task. Obviously: $f_1 \neq f_2 \neq \ldots f_N$. We propose:

$$f_i = f_{y-x} \text{sen}(\alpha_i) \cos(\beta_i) \tag{16}$$

where f_{y-x} is the average resistance force of the average segment in the y–x plane, α_i is the angle between the stress direction projected on the y–x plane and the direction of the ith segment in the y–x plane and β_i is the angle between the y–x plane and the stress direction. If the segments are considered randomly oriented in the y–x plane, the same amount of segments can be found in any direction within this plane. In addition, if the y–x plane is deviated certain angle respect to the stress direction, all segments present the same angle between the stress direction and the y–x plane. Then, $\alpha_1 \neq \alpha_2 \neq \ldots \alpha_N$ and $\beta_1 = \beta_2 = \ldots \beta_N = \beta$. Fig. 6 may be useful to visualize this argument. It is important to mention that the argument was explained considering that the compression force is applied in direction parallel to the molding plane.

Furthermore, replacing f_i of Eq. (15) by Eq. (16) and replacing the sum over the sinus by N times the average sinus evaluated for angles between 0 and $\pi/2$ gives:

$$F = 0.64\, N f_{y-x}\ \cos(\beta) \tag{17}$$

In consequence, the force capable to resist an average segment in the model network is:

$$F = F\, N^{-1} = 0.64\ \cos(\beta) f_{y-x} \tag{18}$$

The segments are slender enough to consider buckling effects under compression. In fact, the geometrical slenderness (s) of the segments can be calculated as the ratio between the length (L = 0.007 m) and the smallest dimension of its transversal section (e = 0.0002 m). In our case: s = 36 justifying the consideration of buckling effects of the segments of the network under compression. The critical load for buckling adapted to our case is given by the Euler's formula:

$$f_{y-x} = \pi^2 E_s I K^{-2} L^{-2} \tag{19}$$

K is the segment effective length factor and depends on the conditions of the end supports of the segments. Introducing Eq. (19) in Eq. (18), dividing by the transversal area of the strand and rearranging, Eq. (20) is obtained:

$$\sigma_{f,s} = 0.64 \cos(\beta) \pi^2 I E_s a^{-1} K^{-2} L^{-2} \tag{20}$$

Finally, $\sigma_{//}^{crush}$ is obtained introducing Eq. (20) into Eq. (2):

$$\sigma_{//}^{crush} = 0.65\ V_s^{1.5} 0.64\ \cos(\beta) \pi^2 I E_s a^{-1} K^{-2} L^{-2} \tag{21}$$

Following the same procedure, $\sigma_{\perp}^{crush}$ is obtained as:

$$\sigma_{\perp}^{crush} = 0.65\ V_s^{1.5}\ 0.64\ \cos(\beta) \pi^2 I E_s a^{-1} K^{-2} L^{-2} \tag{22}$$

The elasticity modulus of the model network (E_n) is calculated as the ratio between σ^{crush} and ε^{crush}. It is important to be noted that $E_n \neq E_s$. And the elasticity modulus of the WWCC is calculated according to Eq. (1):

$$E_{//}^{wwcc} = \sigma_{//}^{crush}\ V_s^2\ \varepsilon_{//}^{crush-1} \tag{23}$$

Following the same procedure, $E_{\perp}^{wwcc}$ is obtained as:

$$E_{\perp}^{wwcc} = \sigma_{\perp}^{crush}\ V_s^2\ \varepsilon_{\perp}^{crush-1} \tag{24}$$

Finally, σ^{coll} is obtained according to Eq. (3):

$$\sigma_{//}^{coll} = 0.05 \sigma_{//}^{crush}\ V_s^2\ \varepsilon_{//}^{crush-1} \tag{25}$$

Eqs. 21–24 describe the mechanical behavior of WWCC under compression parallel and perpendicular to its molding plane.

4.6. Summary of raw experimental data

For easy reading, a summary of experimental data is presented. Those data are required to solve Eqs. 21–24. The average length (L), the average transversal area (a) and the average moment of inertia (I) of the segments are assumed to be equal to the strand gap between the bonds with other strands, the transversal area and the moment of inertia of the strands. Then: L = 0.007 m, a = 3.56 10^{-6} m^2 and I = 1.85 10^{-15} m^4, respectively.

In our case, K is 0.5 since all the segments can be considered as firmly supported by nodes at both ends. E_s is the average elasticity modulus of the strands which can be estimated according to the Reuss and Voigt models of Eqs. (4) and (5). Using the values for E_w = 1500 MPa, E_c = 18,400 MPa, V_w = 0.7 and V_c = 0.3 obtained in precedent sections, E_s^{Reuss} and E_s^{Voigt} resulted 2200 MPa and 6600 MPa, respectively. The deviation of the y–x plane respect to the direction of the compressive force in the model network is equivalent to the angle between the plane where strands lies 2D randomly oriented and the direction of the applied compressive force: β = 0.17 rads. Finally, V_s results 0.4.

4.7. Model results and comparison with experimental values

Eqs. (21) and (22) were solved using the value parameters listed in the precedent section. In principle, E_s has two possible values: E_s^{Reuss} and E_s^{Voigt}. Therefore, $\sigma_{//}^{crush\ (Reuss)}$, $\sigma_{//}^{crush\ (Voigt)}$, $\sigma_{\perp}^{crush\ (Reuss)}$ and $\sigma_{\perp}^{crush\ (Voigt)}$ were calculated and resulted: 0.096 MPa, 0.289 MPa, 0.016 MPa and 0.050 MPa, respectively. Those values were compared with the experimental values: $\sigma_{//}^{crush}$ = 0.100 MPa and $\sigma_{\perp}^{crush}$ = 0.043 MPa. The sandwich structure of wood and cement behaves mainly according to the Reuss model if the stress is applied in the direction parallel to the molding plane and mainly according to the Voigt model if the stress is applied in the direction perpendicular to the molding plane. The real situation would not be pure Reuss or Voigt, but a mixture of both.

Subsequently, $E_{//}$ and $E_{\perp}$ were calculated according to Eqs. (23) and (24) and using $\sigma_{//}^{crush\ (Reuss)}$ and $\sigma_{\perp}^{crush\ (Voigt)}$, respectively. Finally, $\sigma_{//}^{coll}$ was calculated according to Eq. (25) and using $\sigma_{//}^{crush\ (Reuss)}$. Table 7 presents the results of the proposed hierarchical model of WWCC and the corresponding averaged experimental values.

4.8. Verification of the model in other WWCC conditions

The verification of the model in other WWCC conditions is discussed using data that can be easily calculated from raw materials. The reason for this is to certify the validity of the model under

Table 8
Validation of the model in other WWCC conditions.

	WW/PC = 0.250		WW/PC = 0.500		Doubled molding volume	
Parameter	Model MPa	Experimental MPa	Model MPa	Experimental MPa	Model MPa	Experimental MPa
$\sigma_{//}^{crush}$	0.167	0.170	0.070	0.069	0.016	0.018
$\sigma_{\perp}^{crush}$	0.060	0.078	0.019	0.028	0.016	0.015
$E_{//}$	1.843	1.503	0.470	0.550	0.035	0.045
$E_{\perp}$	0.660	0.677	0.125	0.165	0.035	0.026

practical application conditions where accuracy is usually sacrificed in terms of speed and ease of calculation.

The variation of the WW/PC ratio is expected to affect V_s because a different amount of solid materials is cast in the same molding cavity. The decrease of WW/PC from 0.375 to 0.250 by the increment of the amount of PC from 1200 g to 1800 g, and corresponding amounts of $CaCl_2$ and H_2O, generates an extra of 441 cm^3 of set PC in the mold. Oppositely, the increment of WW/PC from 0.375 to 0.500 by the decrease of the amount of PC from 1200 g to 900 g, and corresponding amounts of $CaCl_2$ and H_2O, generates a lack of 217 cm^3 of set PC in the mold. Therefore, $V_s = 0.47$ when WW/PC = 0.250 and $V_s = 0.37$ when WW/PC = 0.500. Moreover, the variation of the WW/PC ratio is expected to affect V_w and V_c because of the changes in the relative proportions of WW and PC. Here, as the amount of WW remained unchanged at 450 g, V_w and V_c can be calculated as 0.46 and 0.54, respectively when WW/PC = 0.250, and 0.78 and 0.22, respectively when WW/PC = 0.500. These changes propagate to E_s according to Eqs. (4) and (5). The detachment of the WW/PC interface and cracking of the PC coating on the wood surface mechanisms responsible for the ultimate resistance for crushing are considered unaltered by the variation of the WW/PC ratio. Therefore, ε^{crush} is assumed unchanged. Finally, the modified V_s and E_s affect the $\sigma_{//}^{crush}$, $\sigma_{\perp}^{crush}$, $E_{//}$ and $E_{\perp}$ according to Eqs. 21–24, respectively. Insignificant variations are assumed for β, I, K, a and L since the geometry of the strands, the amount of wood, the molding volume and the operative procedure were not modified.

The variation of the molding volume is expected to affect V_s, β and L. The increment of the molding volume from 6300 cm^3 to 12,600 cm^3 keeping constant the total amount of raw materials decreases V_s from 0.42 to 0.21. In addition, as the total amount of WW is preserved, L shall be increased to allow the same amount of material to fill the double of volume. Then, L is expected to increase from 0.007 m to 0.014 m. Finally, visual appreciation of the specimens reveals that the strands are randomly oriented in all directions. Practically no differences can be observed in the // and $\perp$ directions of the specimens. Therefore, the material is expected to decrease the high anisotropy observed when raw materials are pressed down in a reduced volume. Therefore, β is assumed to change from 0.17 rads to 0.79 rads. Thus, $\sin(\beta) = \cos(\beta)$. Finally, the modified V_s, β and L affect the $\sigma_{//}^{crush}$, $\sigma_{\perp}^{crush}$, $E_{//}$ and $E_{\perp}$ according to Eqs. 21–24, respectively. Insignificant variations are assumed for E_s, I, K and a since the geometry of the strands and the WW/PC ratio were not modified. Table 8 can be used for detailed comparison between model and experimental results. Evidently, the model responds well to the explored conditions.

5. Conclusions

The hierarchical model 3D open cellular structured material, 2D randomly oriented segment-nodes network and the sandwich structure of wood and cement composites is capable to model the mechanical behavior of the complex WWCC structure. The failure mechanism of WWCC under compressive strength is the buckling of the slender sandwich structures of wood and cement. If the direction of compression is parallel to the molding plane the sandwich structure of wood and cement behaves mainly according to the Reuss model. Oppositely, if the direction of compression is perpendicular to the molding plane the sandwich structure of wood and cement behaves mainly according to the Voigt model.

Acknowledgments

The authors thank to Father Atilio Rosso for his guidance and advise and to the Secretaría de Estado de Ciencia Tecnología e Innovación Productiva of the Santa Fe Province and Cerámica Litoral for the financial support.

References

[1] Vasiliev VV, Morozov EV. Mechanics and analysis of composite materials. 1th ed. Amsterdam: Elsevier; 2001.
[2] Cox B, Yang Q. In quest of virtual tests for structural composites. Science 2006;314:1102–7.
[3] Frybort S, Mauritz R, Teischinger A, Muller U. Cement bonded composites – a mechanical review. BioResources 2008;3:602–26.
[4] Jorge FC, Pereira C, Ferreira JMF. Wood–cement composites: a review. Holz als Roh – und Werkstoff 2004;62:370–7.
[5] Wolfe R, Gjinolli A. The use of recycled wood and paper in building applications. Madison: Wiscosin; 1996.
[6] Moslemi AA. Adv Perform Mater 1999;6:161–79.
[7] Simatupang MH, Geimer R. 3rd International Inorganic-Bonded Wood and Fiber Composite Materials. Washington, USA; 1992: 114–20.
[8] Lee AWC. Physical and mechanical properties of cement bonded southern pine excelsior board. Forest Prod J 1984;34:30–4.
[9] Sierra Beltran MG, Schlangen E. Wood fibre reinforced cement matrix: a micromechanical based approach. Key Eng Mater 2008;385:445–8.
[10] Wei YM, Guang Zhou Y, Tomita B. Hydration behavior of wood cement-based composite I: Evaluation of wood species effects on compatibility and strength with ordinary Portland cement. J Wood Sci 2000;46:296–302.
[11] Pehanich JL, Blankenhorn PR, Silsbee MR. Wood fiber surface treatment level effects on selected mechanical properties of wood fiber-cement composites. Cem Conc Res 2004;34:59–65.
[12] Coutts RSP, Warden PG. Effect of compaction on the properties of air-cured wood fibre reinforced cement. Cem Concr Compos 1990;12:151–6.
[13] Ashori A, Tabarsa T, Sepahvand S. Cement-bonded composite boards made from poplar strands. Constr Build Mater 2012;26:131–4.
[14] Gibson LJ, Ashby MF. Cellular Solids. 1th ed. Cambridge: UK; 1988.
[15] Paul B. Prediction of elastic constants of materials. Trans. AIME1960; 218: 36–41.
[16] Fratzl P, Weinkamer R. Prog Mater Sci 2007;52. 1263-34.
[17] Haecker CJ, Garboczi EJ, Bullard JW, Bohn RB, Sun Z, Voigt T. Modeling the linear elastic properties of Portland cement paste. Cem Concr Res 2005;35:1948–60.
[18] Smilauer V, Bittnar Z. Microstructure-based micromechanical prediction of elastic properties in hydrating cement paste. Cem Concr Res 2006;36:1708–18.
[19] Diaz BG, Otaño ME, Keil GD, Peri P, Andia I. Propiedades de las maderas Argentinas. Buenos Aires: INTA BI 16; 1990.
[20] Technical brochure. CPN40 IRAM 50.000. www.minetti.com.ar 01/02/2010.
[21] Technical brochure. Paraffin. www.induquimika.com.ar 05/02/2010.
[22] Karade SR, Irle M, Maher K. Assessment of wood–cement compatibility: a new approach. Holzforschung 2003;57:672–80.
[23] Building Code Requirements for Structural Concrete and Commentary. American Concrete Institute. ACI Committee ACI 318–08: ISBN 0870312642. 2008.